Supplementary Information (SI) for Materials Chemistry Frontiers.

Supporting Information

Probing Biomass Mimic Guaiacol Confinement and Interactions in ZSM-5 Zeolite

Kyle A. Watson,[a] Ming-Feng Hsieh,[b] Stephen Day,[c] Luke Tuxworth,[b] and Frédéric Blanc[a,d,e]*

[a] Department of Chemistry, University of Liverpool, Liverpool L69 7ZD, UK

[b] Johnson Matthey Technology Centre, Billingham TS23 1LB, UK

[c] Johnson Matthey Technology Centre, Sonning Common RG4 9NH, UK

[d] Stephenson Institute for Renewable Energy, University of Liverpool, Liverpool L69 7ZF, UK

[e] Leverhulme Research Centre for Functional Materials Design, University of Liverpool, Liverpool L7 3NY, UK

* Corresponding author's email: frederic.blanc@liverpool.ac.uk

Experimental Section

Sample Preparation

Guaiacol (99+%) and silicon carbide (SiC) powder (100 %, particle size = 340 µm) were purchased from ThermoFischer Scientific. 60% ^{17}O enriched O_2 gas was obtained from Isotec. ZSM-5 (SiO_2/Al_2O_3 = 34, particle size < 5 µm) was supplied by Johnson Matthey.

Guaiacol adsorbed ZSM-5 was prepared at room temperature by adding guaiacol (ranging from 4.5-45.0 µL) dropwise over 10 seconds to ZSM-5 (200 mg) in a vial and then shaken to ensure homogenisation. Guaiacol loadings were chosen corresponding to 10, 25, 50 and 100 % of the volume employed for the pyrolysis activation process. Ar gas adsorption for Am-NatA-ZSM-5 (Table S3) report a pore volume of 0.24 cm^3g^{-1}; based on this pore volume, the guaiacol loadings correspond to 9, 23, 47 and 94% of the theoretical pore volume, respectively.

Guaiacol activated ZSM-5: Under air, ZSM-5 (200 mg) and SiC (400 mg) were layered in a quartz tube on top of a built-in sintered quartz disc, then placed within a furnace which temperature was ramped from room temperature to 500 or 600 °C (see below) at 10 °C/min. ZSM-5 was first heated at target temperature for 45 min to dehydrate under air before Ar gas was flowed through the tube at 425 mL/min for 15 min. Guaiacol (50 mg, 45 µL, 1:4 guaiacol:ZSM-5 weight ratio) was injected with a micro-syringe into the Ar gas flow on top of the reactor. After the desired collection period (30-60 seconds), the furnace heating elements were then withdrawn allowing the sample to cool quickly to approximately 60 °C in under an estimated 30 s. The flow of Ar gas was then discontinued, and the sample collected and sieved to separate the post-reaction ZSM-5 from the SiC particles. Reaction products are collected in a vial at the end of the reactor brought to low temperatures in an ice bath.

Dehydrated ZSM-5 was obtained by heating under dynamic vacuum at 10 mbar using the following temperatures that minimise dealumination:[1] ZSM-5 was heated at 1 °C/min to 50 °C and then held for 1 hour, then ramped to 100 °C and held for 1 hour and finally ramped to 300 °C and held for 10.5 hours. The samples were then isolated at 300°C and allowed to cool naturally in the furnace to room temperature under static vacuum. Samples were packed in a MBraun LabMaster 130 glovebox (O_2, $H_2O \leq 1.0$ ppm) under an Ar atmosphere.

^{17}O enriched ZSM-5 was prepared by exposing dehydrated ZSM-5 (as described above) to 60% ^{17}O enriched O_2 gas in a closed quartz tube heated to either 300, 500 or 700 °C for 16 hours at a heating ramp rate of 1 °C/min. After the heating period, the tube was allowed to cool naturally in the furnace to room temperature.

Solid State NMR Spectroscopy

NMR experiments were recorded at various field strengths on a number of spectrometers as indicated. Experiments at 9.4 T used a Bruker Avance III HD spectrometer with a Bruker 4 mm HXY MAS probe in double resonance (DR) mode, at 18.8 T a Bruker Avance NEO spectrometer equipped with a Bruker 1.3 mm HXY MAS probe in DR mode, at 20.0 T a Bruker Avance NEO spectrometer with a Bruker 3.2 mm HXY MAS probe in DR mode, a 23.5 T a Bruker Avance NEO spectrometer with a Bruker 3.2 mm HX MAS probe.

1D ^1H NMR spectrum of neat guaiacol were obtained under MAS at 220 Hz at 9.4 T with the one pulse experiment. The ^1H MAS spectra of ambient moisture ZSM-5, guaiacol adsorbed ZSM-5 and guaiacol activated ZSM-5 were obtained at 18.8 T under MAS at 60 kHz with the Hahn echo experiment (10 rotor periods were used to reduce the ^1H background signal). The ^1H MAS spectra

of dehydrated ZSM-5 were obtained at 20.0 T under MAS at 16 kHz with the Hahn echo experiment (4 rotor periods to reduce ^{1}H background signal). ^{1}H NMR experiments used an experimentally optimised flip angle of 90° with a pulse duration of 5.0 µs at a radiofrequency (rf) amplitude of 50 kHz (with the exception of Am-NatA-ZSM-5 and the ZSM-5 samples with various amount of guaiacol adsorbed in Figure 1 which used an experimentally optimised flip angle of 90° with a pulse duration of 2.0 µs at a rf amplitude of 125 kHz). All 1D ^{1}H NMR experiments used a recycle delay of 5 × T_1 (4-20s dependant on sample) for quantitative measurements. T_1 values were determined by saturation recovery experiments performed with a saturation block consisting of a train of 100 pulses separated by a delay of 1 ms. The resulting normalised data were fit using the equation

$$I(t) = 1 - \exp\left[-\left(\frac{\tau_1}{T_1}\right)^{\alpha_1}\right] \quad (1)$$

where $I(t)$ is the magnetization at time t, τ_1 the variable delay for magnetization build up and α_1 the stretch exponential to account for a distribution of values. T_2 values were determined by performing a series of Hahn echo experiments with increasing rotor-synchronised echo delays. The resulting normalised data were fit using the equation

$$I(t) = \exp\left[-\left(\frac{\tau_2}{T_2}\right)^{\alpha_2}\right] \quad (2)$$

where $I(t)$ is the magnetization at time t, τ_2 the variable echo delay and α_2 the stretch exponential to account for a distribution of values.

A ^{1}H 2D Exchange SpectroscopY (EXSY) NMR spectrum[2] was obtained at 18.8 T under MAS at 60 kHz. Pulses were used with an experimentally optimised flip angle of 90° with a duration of 2.0 µs at a rf amplitude of 125 kHz. 4096 rotor-synchronized t_1 increments (1 rotor period) and a mixing time of 20 ms were used. A recycle delay of 1.3 × T_1 was used to maximise signal to noise per unit time.

^{1}H -^{13}C Cross-Polarization CP MAS NMR and heteronuclear correlation (HETCOR) experiments were obtained at 9.4 T under MAS at 10 kHz. The ^{1}H 90° pulse had a duration of 3.6 µs at a rf field amplitude of 70 kHz. For CP, a ^{1}H rf field amplitude of 60 kHz was used for with a ramped 70-100% pulse on ^{1}H to match the Hartman-Hahn condition of ^{13}C at a rf field amplitude of 47 kHz. SPINAL64 heteronuclear decoupling[3] was used at a rf field amplitude of 70 kHz. A recycle delay of 1.3 × T_1 on ^{1}H was used to maximise signal to noise per unit time. For the HETCOR experiment, 16 rotor-synchronized t_1 increments (1 rotor period) were used. The ^{13}C NMR spectrum of neat guaiacol was obtained at 9.4 T under static conditions and direct ^{13}C excitation with continuous wave ^{1}H decoupling experiment during detection. An experimentally optimised flip angle of 90° of 5.0 µs at a rf amplitude of 50 kHz was used on ^{13}C. Continuous wave ^{1}H decoupling was used at a rf field amplitude of 40 kHz.

^{17}O MAS spectra were obtained at 9.4 T, 18.8 T and 20.0 T under MAS at 10, 16 and 20 kHz, respectively. The spectra were obtained using a Hahn echo (1 rotor period) pulse sequence at 9.4 T and 18.8 T and a one pulse experiment at 20.0 T. Experiments at 9.4 T and 20.0 T used optimised flip angles of 90° with pulse durations of 1.67 µs at a rf amplitude of 50 kHz, with experiments at 18.8 T using a pulse duration of 2.4 µs at a rf amplitude of 35 kHz. All experiments used a recycle delay of 5 × T_1 (10 s) for quantitative measurements with T_1 determined by saturation recovery experiments and fitted using equation 1 as described above for ^{1}H.

2D ^{17}O multiple-quantum magic angle spinning (MQMAS)[4] experiments were conducted at 9.4 T under MAS at 10 kHz with a z-filter pulse sequence.[5] A rf field amplitude of 100 kHz for the optimised excitation (4.0 μs) and reconversion pulses (1.5 μs) and a rf field amplitude of 10 kHz for the 90° central transition selective pulse (8.33 μs) were used. 36 rotor synchronized (1 rotor period) t_1 increments were used with a recycle delay of 0.2 s to maximize signal to noise per unit time. The isotropic chemical shifts (δ_{CS}) were determined by extracting the position of the centre of gravity of the resonances projected along the isotropic (δ_1) and anisotropic (δ_2) dimensions of the sheared MQMAS spectra using equation 1.[6]

$$\delta_{CS} = \frac{17\delta_1 + 10\delta_2}{27} \quad (3)$$

1D ^{17}O MAS spectra were then fitted with the line shape analysis tool "Sola" in Topspin 4.4.0, to extract the relevant quadrupolar coupling (C_Q) and electric field gradient tensor asymmetry parameters (η_Q).

2D ^{1}H-^{17}O dipolar heteronuclear multiple-quantum coherence (D-HMQC) experiments were conducted at 23.5 T under MAS at 16 kHz using the SR4$^2_1$ recoupling sequence on ^{1}H.[7] For ^{1}H, pulse durations of 3.75 and 7.5 μs at a rf amplitude of 66.7 kHz were used for experimentally optimized 90° and 180° pulses, respectively. SR4$^2_1$ recoupling pulses on ^{1}H used a rotor-synchronized pulse length of 15.62 μs (1/4 of a rotor period) at a rf field amplitude of 32 kHz as required to match the condition to be 2 × MAS rate. For ^{17}O, pulse durations of 13.9 μs at a rf amplitude of 6 kHz were used for central transition selective pulses. 24 rotor-synchronized t_1 increments (1 rotor period) increments were used with a ^{1}H recycle delay of 1.3 × T_1. Recoupling times from 0.75 to 6.0 ms were used to estimate strength of ^{1}H-^{17}O dipolar coupling constants.

^{27}Al and ^{29}Si MAS spectra were obtained at 9.4 T under MAS at 10 kHz. ^{27}Al and ^{29}Si spectra were obtained with the one pulse experiment using experimentally optimised flip angles of 90° of pulse durations of 2.1 μs at a rf amplitude of 40 kHz and 6.2 μs at 40 kHz, respectively. All ^{27}Al and ^{29}Si experiments used a recycle delay of 5 × T_1 (0.1 and 60 s respectively) for quantitative measurements. For ^{27}Al the recycle delay was found to be sufficient for quantitative experiments at 0.1 s and no further measurements were taken. For ^{29}Si the T_1 was measured by saturation recovery experiments and fitted using equation 1 as described above for ^{1}H.

Shifts for ^{17}O and ^{27}Al are quoted in ppm relative their primary references of water for ^{17}O (0 ppm) and 1.1 M $Al(NO_3)_3$ in D_2O for ^{27}Al (0 ppm). These were also used for the rf calibration of these quadrupolar nuclei. Chemical shifts for ^{1}H, ^{13}C and ^{29}Si are quoted in ppm relative to their secondary references of adamantane for ^{1}H (1.8 ppm) and ^{13}C (29.45 ppm)[8] and to octakis(trimethylsiloxy)silsesquioxane (Q8M8) for ^{29}Si (11.5 ppm)[9]. ^{1}H, ^{13}C and ^{29}Si are all relative to 0 ppm of their primary reference tetramethylsilane (TMS).

Numerical Simulations

Simulations of the ^{1}H-^{17}O D-HMQC signal build-up were performed using the SIMPSON simulation package.[10] The SR4$^2_1$ recoupling sequence was implemented as described in the literature,[11] which was modified to reproduced the experimental conditions described above. Powder averaging was carried with the γ compute method with 4180 molecular orientations α_{MR} β_{MR} using the ZCW algorithm[12] and stepping the Euler angle γ_{MR} over 100 steps. Build-up curves were calculated for an isolated two-spin ^{1}H-^{17}O system with heteronuclear dipolar coupling constants in the range 100-145 Hz. To assess the influence of homonuclear ^{1}H-^{1}H interactions on the D-HMQC transfer efficiency and capture the presence of other ^{1}H spins,

additional simulations included a third ^{1}H spin dipolar-coupled to the first ^{1}H nucleus was included with a fixed ^{1}H-^{1}H dipolar coupling constant of 300 Hz. The ^{17}O nucleus was treated explicitly using experimentally determined quadrupolar parameters (C_Q = 5.3 MHz and η_Q = 0.15). These simulations estimate a quantitative interpretation of the experimental build-up behaviour in terms of heteronuclear dipolar coupling strengths and the influence of an additional ^{1}H spin.

Liquid State NMR Spectroscopy

^{1}H and ^{13}C NMR spectra of guaiacol in $CDCl_3$ were recorded at 9.4 T using a Bruker Avance III HD spectrometer at room temperature with chemical shifts quoted to the residual protons at 7.26 and 77.2 ppm, respectively.

GC-MS

The guaiacol activation products were dissolved in 1 mL of dichloromethane (DCM). The separation of component products was achieved using a DB-5MS column (30 m × 0.25 mm ID, 0.25 µm film thickness, Agilent Technologies) with a constant flow of 15 mL/min of helium as the carrier gas and with the following temperature program: initial temperature of 50 °C and held for 2 min, increased by 20 °C/min to 300 °C, and held for 2 min. The injection inlet temperature was 250 °C and the injection volume was 1 µL, using a split ratio of 10:1.

The products detection was by a Thermofisher Focus Gas Chromatograph, with ISQ Mass Spec using the following settings: transfer line temperature of 300 °C, source temperature of 300 °C and a solvent delay of 2 min 50 s. Products were identified by retention time and comparison of mass spectra to the National Institute of Standards and Technology (NIST) library.

TGA-MS

The TGA-MS experiments were performed on a Netzsch TG 209 F1 Libra. Each experiment used approximately 10 mg of sample, which was placed in an alumina crucible and heated from 25 °C to 700 °C at a ramp rate of 10 °C/min, in an air stream of 20 ml/min. A slight artificial mass increase (≈ 0.5% of sample mass) is recorded at the beginning of each experiment due to buoyancy effects of the purge gas density decreasing upon heating.

Argon Physisorption

Ar physisorption was conducted using a Micromeritics 3-Flex analyser. Samples were outgassed at 350 °C for 15 hours under vacuum prior to analysis. Apparent Brunauer–Emmett–Teller (BET) surface area was derived using the Rouquerol optimisation method. Micropore volume was obtained using the t-plot method. Mesopore volume is quoted as the difference between the pore volume at last point on the adsorption isotherm (P/Po ~0.995) and the micropore volume as derived from the t-plot.

Additional Data

Table S1. Full list of ZSM-5 samples used with their respective abbreviations.

Full sample description	Abbreviations
Ambient moisture unenriched ZSM-5	Am-NatA-ZSM-5
Guaiacol activated unenriched ZSM-5 (30s collection period)	Act-NatA-ZSM-5
Guaiacol activated unenriched ZSM-5 (300s collection period)	Act300-NatA-ZSM-5
Guaiacol adsorbed ZSM-5 (9% theoretical pore volume filled)	Ads9-NatA-ZSM-5
Guaiacol adsorbed ZSM-5 (23% theoretical pore volume filled)	Ads23-NatA-ZSM-5
Guaiacol adsorbed ZSM-5 (47% theoretical pore volume filled)	Ads47-NatA-ZSM-5
Guaiacol adsorbed ZSM-5 (94% theoretical pore volume filled)	Ads94-NatA-ZSM-5
^{17}O-enriched (500 °C) guaiacol activated ZSM-5	Act-^{17}O(500)-ZSM-5
Dehydrated unenriched ZSM-5	De-NatA-ZSM-5
Dehydrated ^{17}O-enriched ZSM-5 (700 °C)	De-^{17}O(700)-ZSM-5
Ambient moisture ^{17}O-enriched ZSM-5 (300 °C)	Am-^{17}O(300)-ZSM-5
Ambient moisture ^{17}O-enriched ZSM-5 (500 °C)	Am-^{17}O(500)-ZSM-5
Ambient moisture ^{17}O-enriched ZSM-5 (700 °C)	Am-^{17}O(700)-ZSM-5

Table S2: Comparison of guaiacol ^{1}H δ_{CS} and FWHM between guaiacol in $CDCl_3$ (Figure S2), guaiacol neat (Figure 2 a), Ads94-Nat-ZSM-5 and Act-Nat-ZSM-5 (Figure 1 b). T_1 and T_2 values are included for Ads94-Nat-ZSM-5.

		In-pore			Ex-pore				
Guaiacol in $CDCl_3$	δ_{CS} / ppm	-[a]	-[a]	-[a]	3.91 ± 0.01	5.89 ± 0.01	6.91-6.98		7.01-7.05
	FWHM / Hz	-[a]	-[a]	-[a]	1.4 ± 0.1	7.9 ± 0.5	Multiplet		Multi.
Guaiacol Neat (No solvent)	δ_{CS} / ppm	-[a]	-[a]	-[a]	3.0 ± 0.1	-[a]	6.2 ± 0.1	6.3 ± 0.1	6.6 ± 0.1
	FWHM / Hz	-[a]	-[a]	-[a]	20 ± 3	-[a]	24 ± 2	33 ± 4	24 ± 4
Ads94-Nat-ZSM-5	δ_{CS} / ppm	-[a]	3.9 ± 0.1	6.9 ± 0.1	3.1 ± 0.1	-[a]	6.3 ± 0.1	6.4 ± 0.1	6.6 ± 0.1
	FWHM / Hz	-[a]	170 ± 10	350 ± 10	18 ± 1	-[a]	23 ± 4	47 ± 2	24 ± 2
	T_1 / ms	-[a]	90 ± 5	63 ± 3	1294 ± 33	-[a]	1143 ± 100	1424 ± 150	1030 ± 70
	T_2 / ms	-[a]	0.82 ± 0.04	0.81 ± 0.06	18.65 ± 0.83	-[a]	15.31 ± 2.20	11.93 ± 1.50	8.56 ± 1.16
Act-Nat-ZSM-5	δ_{CS} / ppm	2.3 ± 0.1	3.9 ± 0.1	6.9 ± 0.1	-[a]	-[a]	-[a]	-[a]	-[a]
	FWHM / Hz	310 ± 20	240 ± 20	500 ± 20	-[a]	-[a]	-[a]	-[a]	-[a]

[a] Not applicable.

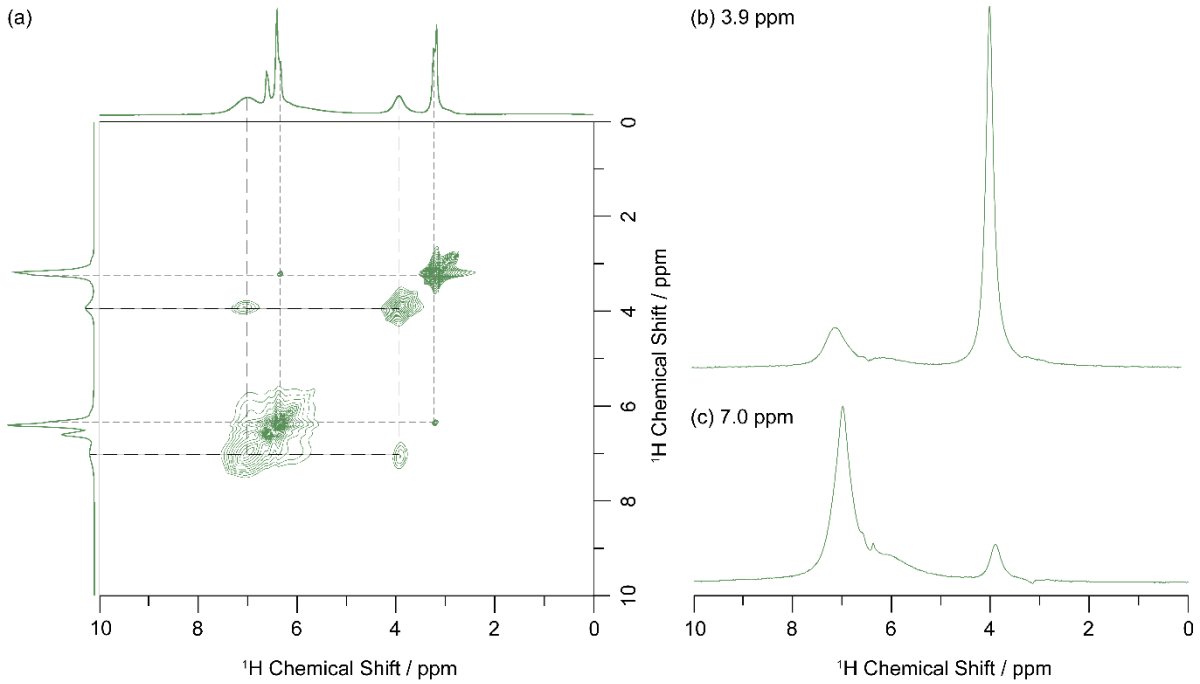

Figure S1. (a) 2D ^{1}H-^{1}H EXSY spectrum of Ads94-Nat-ZSM-5 acquired with a 20 ms mixing time at B_0 = 18.8 T and ν_r = 60 kHz, displaying projections of the 2D spectra along the f_1 (left) and f_2 (top) dimensions. Dashed lines indicate resonances assigned to in-pore guaiacol (black long dashes) and ex-pore guaiacol (grey short dashes). (b,c) 1D spectral slices extracted at f_2 chemical shifts of (b) 3.9 and (c) 7.0 ppm.

Table S3: BET data of AM-Nat-ZSM-5 using Ar adsorption isotherm.

BET area / m^2g^{-1}	Micropore area / m^2g^{-1}	Exterior surface area / m^2g^{-1}	Pore volume / cm^3g^{-1}	Micropore volume / cm^3g^{-1}	Mesopore volume / cm^3g^{-1}
447	404	43	0.24	0.15	0.09

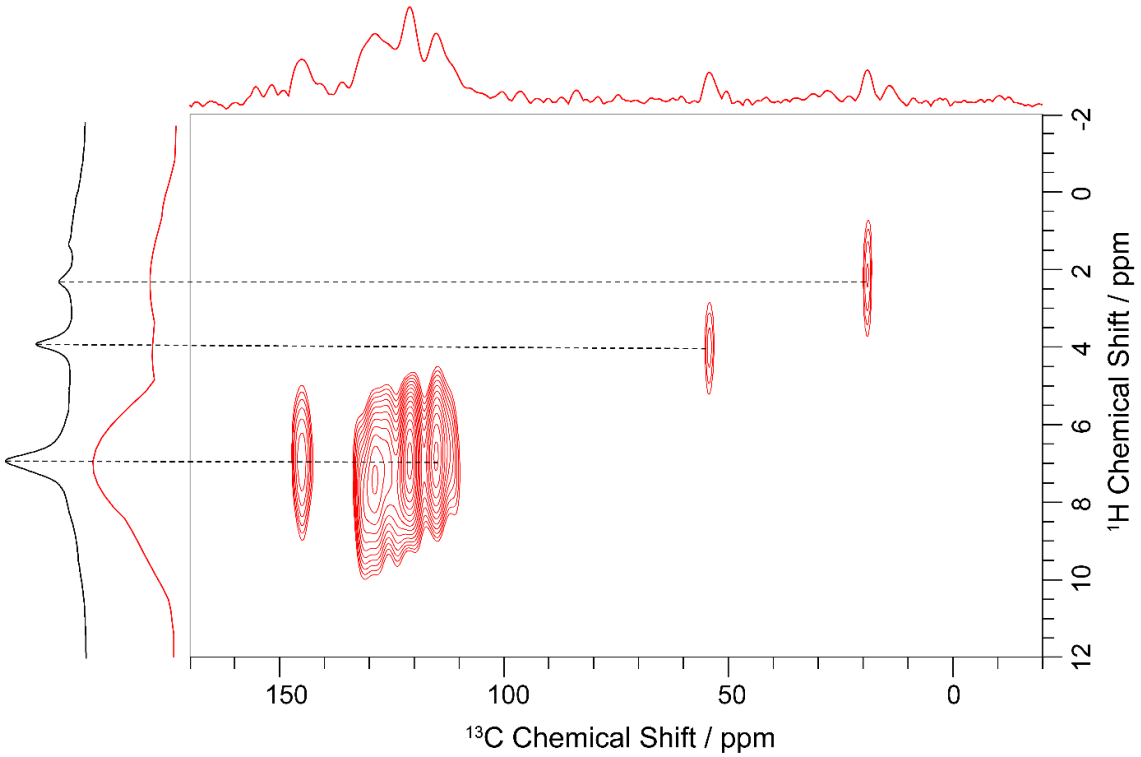

Figure S2. ^{13}C-^{1}H HETCOR of Act-Nat-ZSM-5 recording with a 2 ms contact time at B_0 = 9.4 T and ν_r = 10 kHz. Internal projections (red) are presented with the ^{1}H MAS NMR spectrum (black, Figure 1 g) to guide spectral assignments.

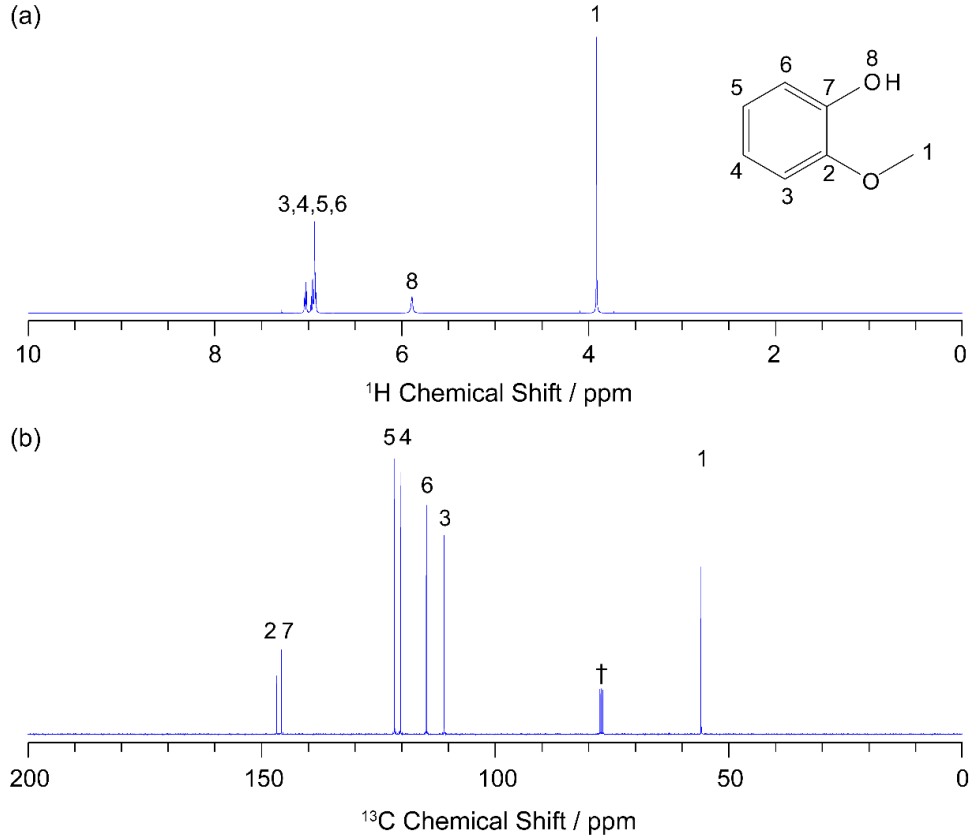

Figure S3. (a) Liquid ^{1}H NMR spectrum and (b) ^{13}C {^{1}H} NMR spectrum of guaiacol in $CDCl_3$. Dagger (†) indicates solvent peak.

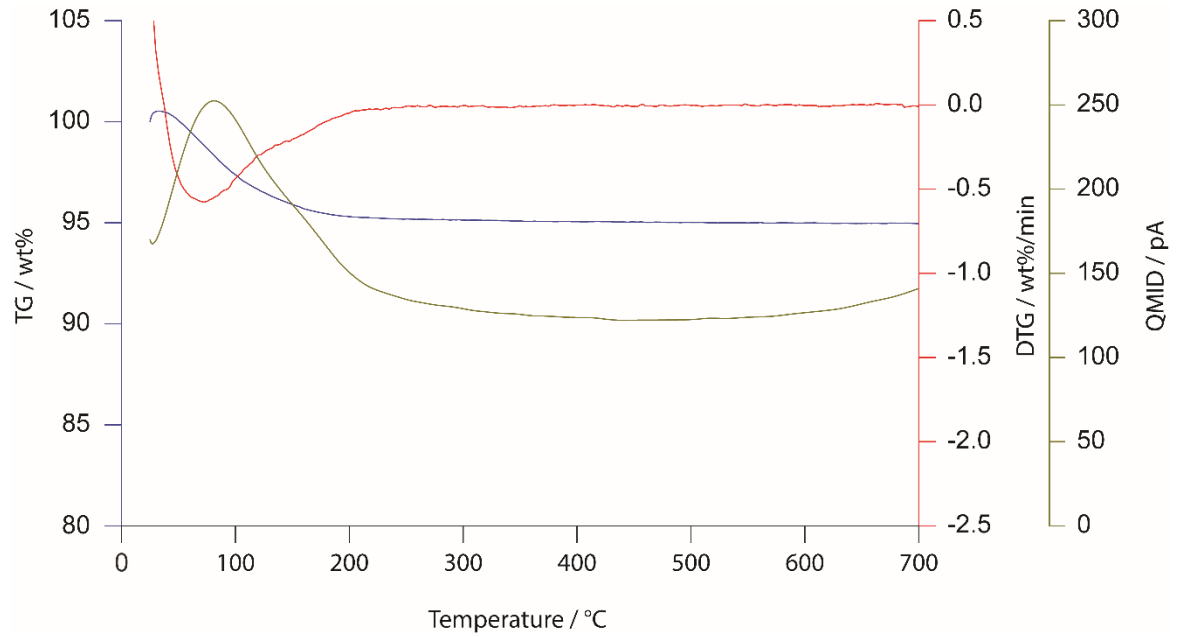

Figure S4. Thermogravimetric analysis of Am-NatA-ZSM-5 with TG (blue), DTG (red) and QMID ion current curve for m/z 18 (olive).

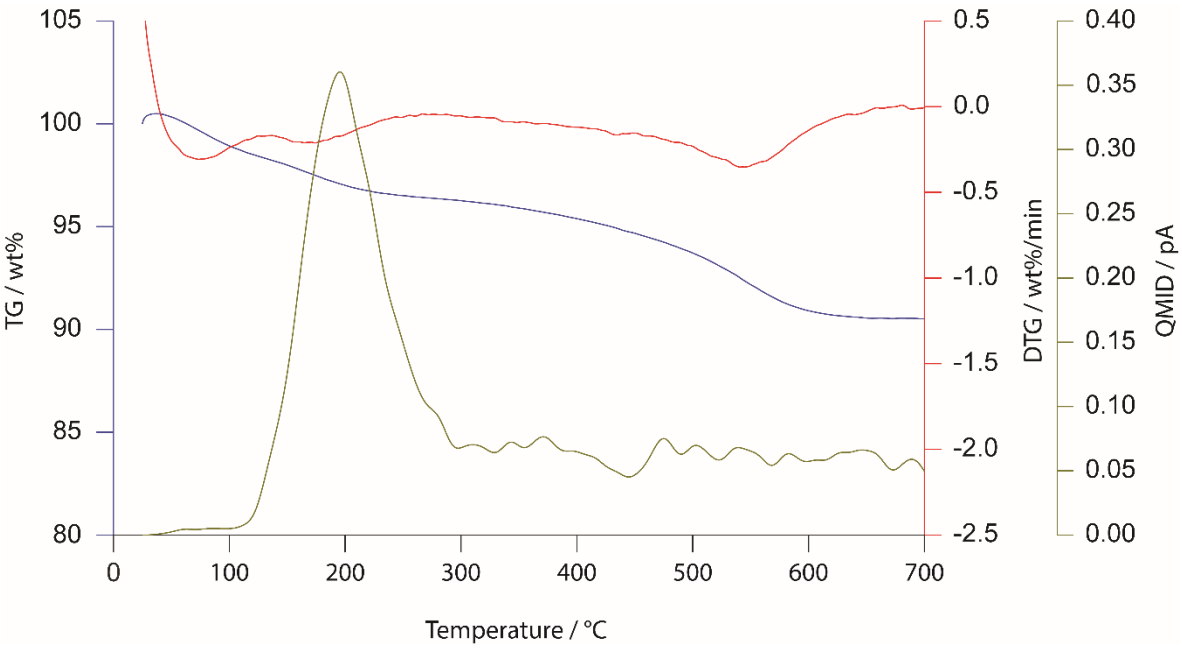

Figure S5. Thermogravimetric analysis of Act-NatA-ZSM-5 with TG (blue), DTG (red) and QMID ion current curve for m/z 124 (olive).

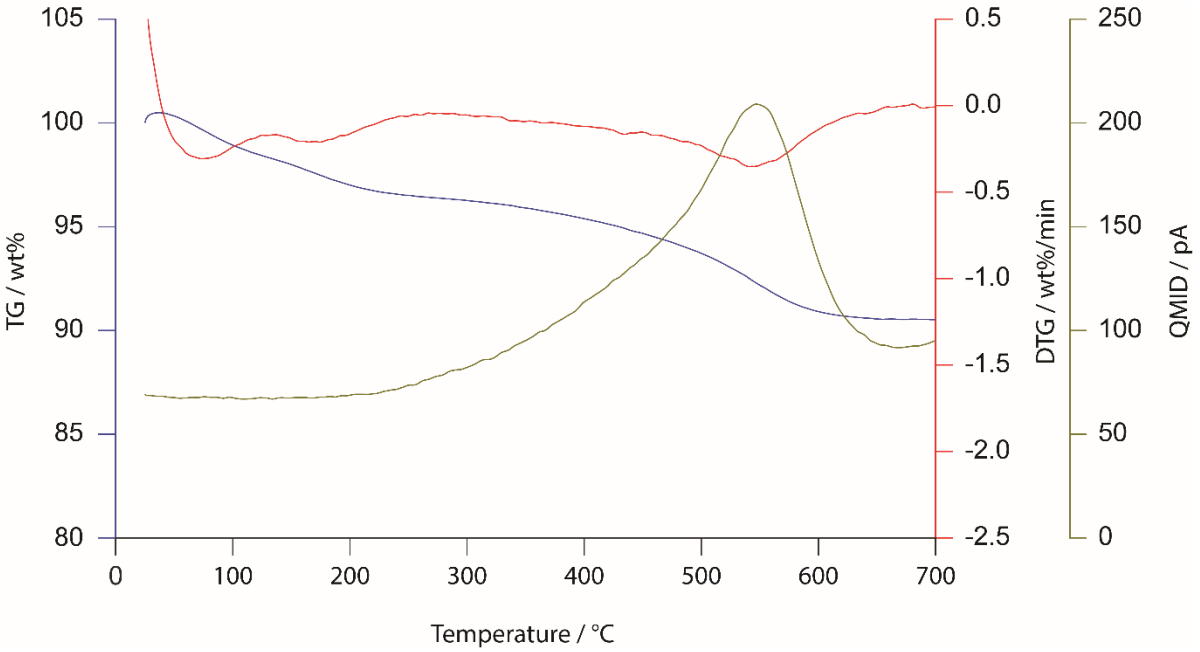

Figure S6. Thermogravimetric analysis of Act-NatA-ZSM-5 with TG (blue), DTG (red) and QMID ion current curve for m/z 44 (olive).

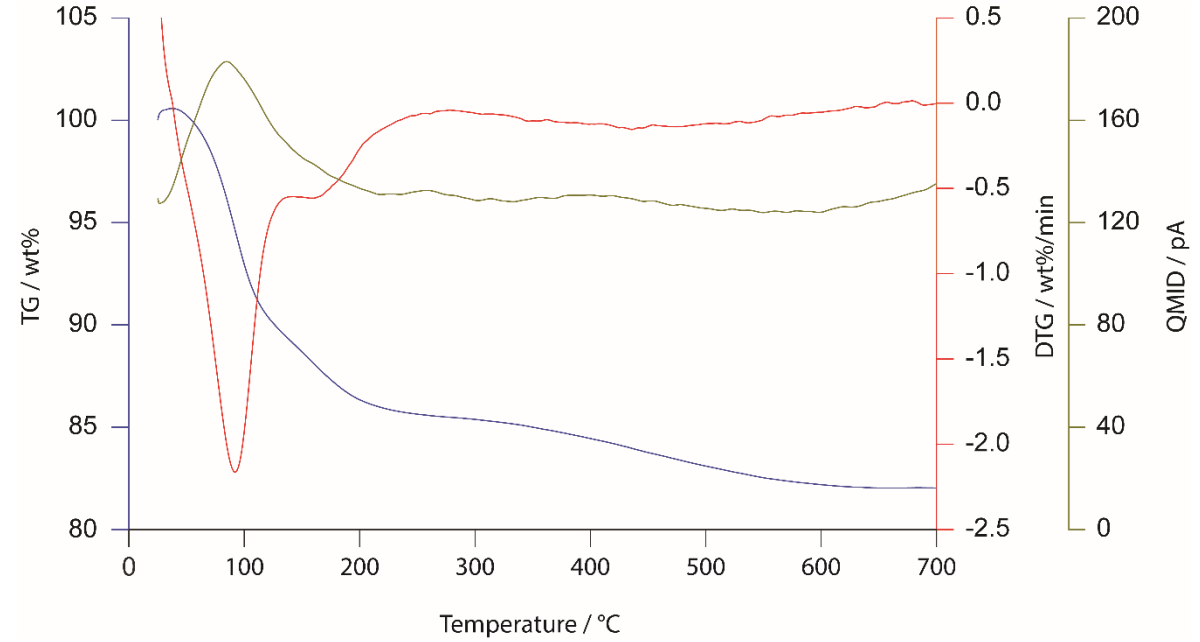

Figure S7. Thermogravimetric analysis of Ads94-NatA-ZSM-5 with TG (blue), DTG (red) and QMID ion current curve for m/z 18 (olive).

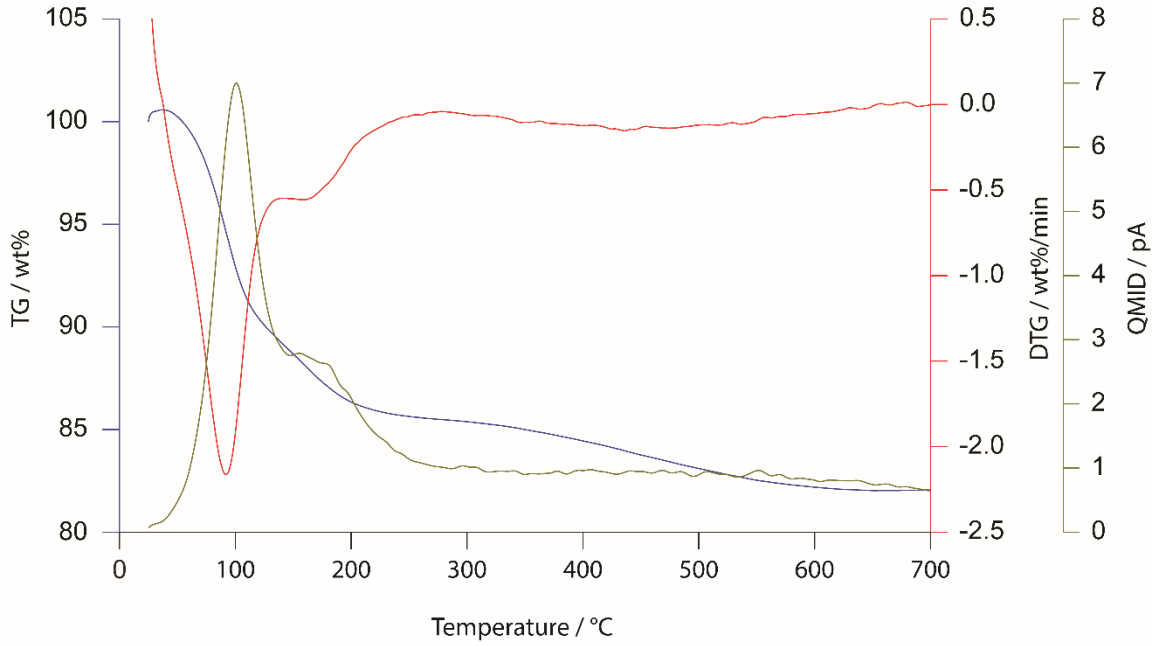

Figure S8. Thermogravimetric analysis of Ads94-NatA-ZSM-5 with TG (blue), DTG (red) and QMID ion current curve for m/z 124 (olive).

Table S4. Products of guaiacol pyrolysis reaction catalysed by Act-^{17}O(500)-ZSM-5 categorised by oxygen content, number of aromatic rings and structural groups expressed as a percentage of peak area of identified peaks. Values are averaged over three reproducible pyrolysis experiments and used to determine the errors.

Oxygen content (peak area% of identified peaks).				
Oxygenated Products / %		Non-Oxygenated Products / %		
52.0 ± 2.7		48.0 ± 2.7		
Number of aromatic rings (peak area% of identified peaks).				
1 ring / %	2 rings / %	3 rings / %	4 rings / %	
53.3 ± 0.9	38.2 ± 0.4	8.3 ± 1.0	0.2 ± 0.1	
Structural composition (peak area% of identified peaks).				
BTEX / %	Phenols / %	Naphthalenes / %	Guaiacol / %	Others / %
12.0 ± 0.7	34.3 ± 0.4	22.0 ± 3.4	0.0	31.8 ± 3.3

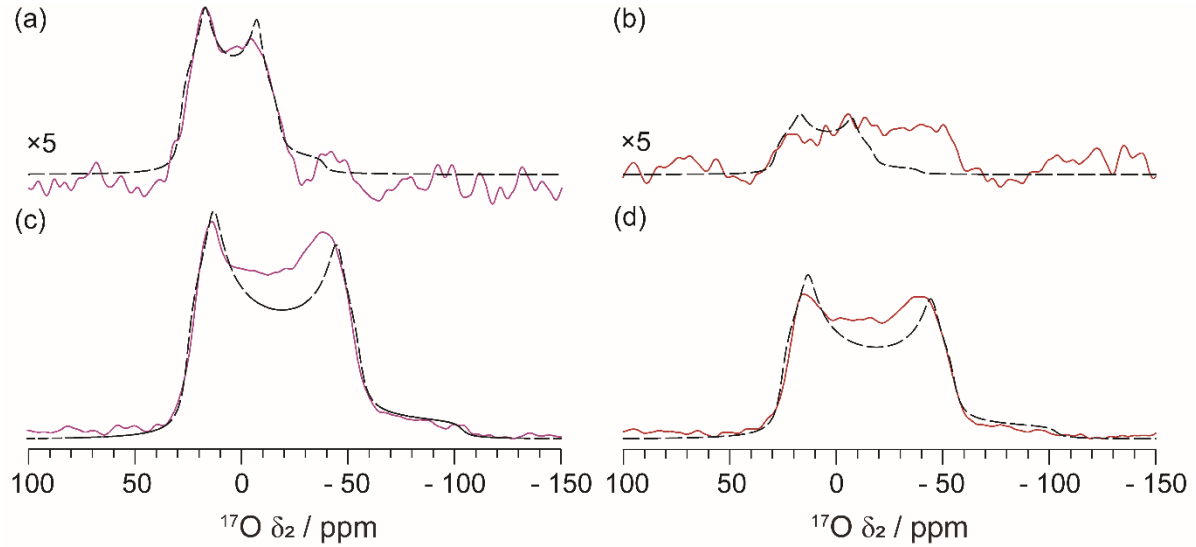

Figure S9. Comparison of the one dimensional ^{17}O MAS NMR line shape at (a,b) δ_1 = 50 ppm (Si-O-Al region) scaled by a factor of 5 and (c,d) δ_1 = 75 ppm (Si-O-Si region) in the ^{17}O MQMAS spectra (Figure 4 c,d) of (a,c, purple) Am-^{17}O(500)-ZSM-5 and (b,d, red) Act-^{17}O(500)-ZSM-5. The experimental spectra are shown as solid coloured lines, with corresponding simulations overlaid as black dashed lines.

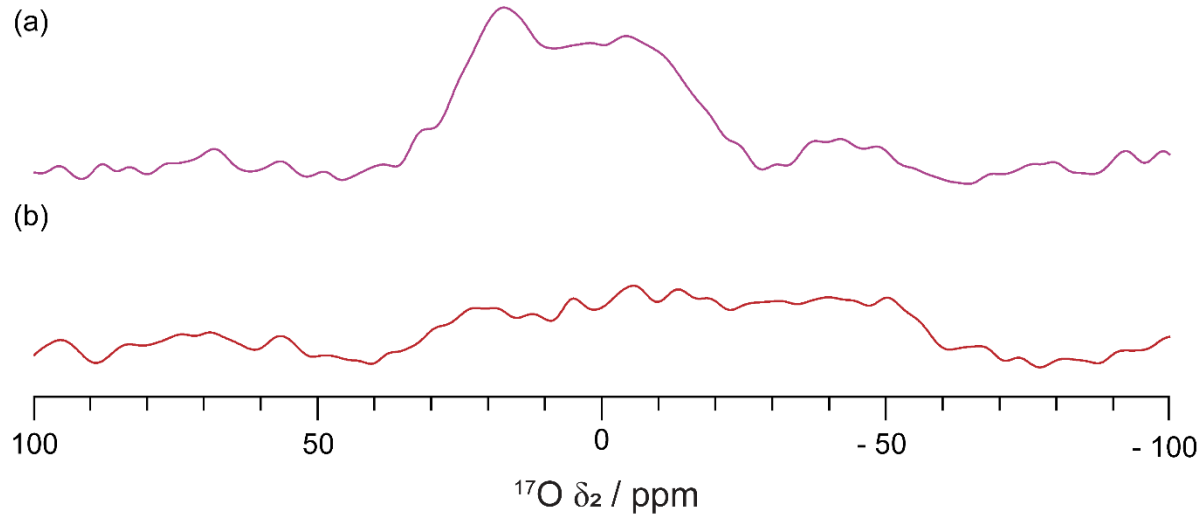

Figure S10. Comparison of the one dimensional ^{17}O MAS NMR line shape at δ_1 = 50 ppm in the ^{17}O MQMAS data (Figure 4 c,d) in the range of the Si-O-Al environment of (a) Am-^{17}O(500)-ZSM-5 and (b) Act-^{17}O(500)-ZSM-5.

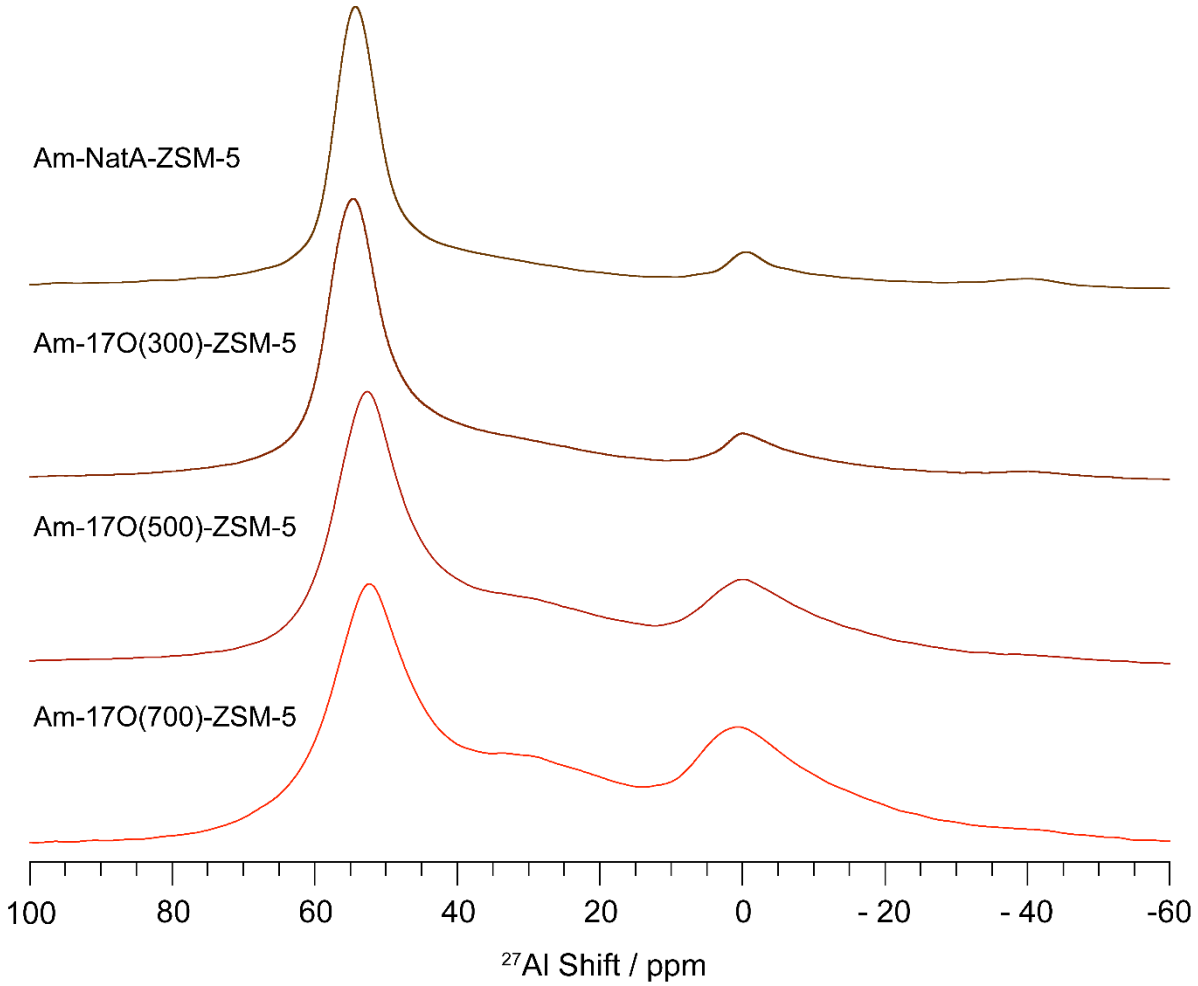

Figure S11. ^{27}Al MAS NMR spectrum of Am-NatA-ZSM-5 and after ^{17}O enrichment at various temperatures as indicated. Data were acquired at B_0 = 9.4 T and with ν_r = 10 kHz.

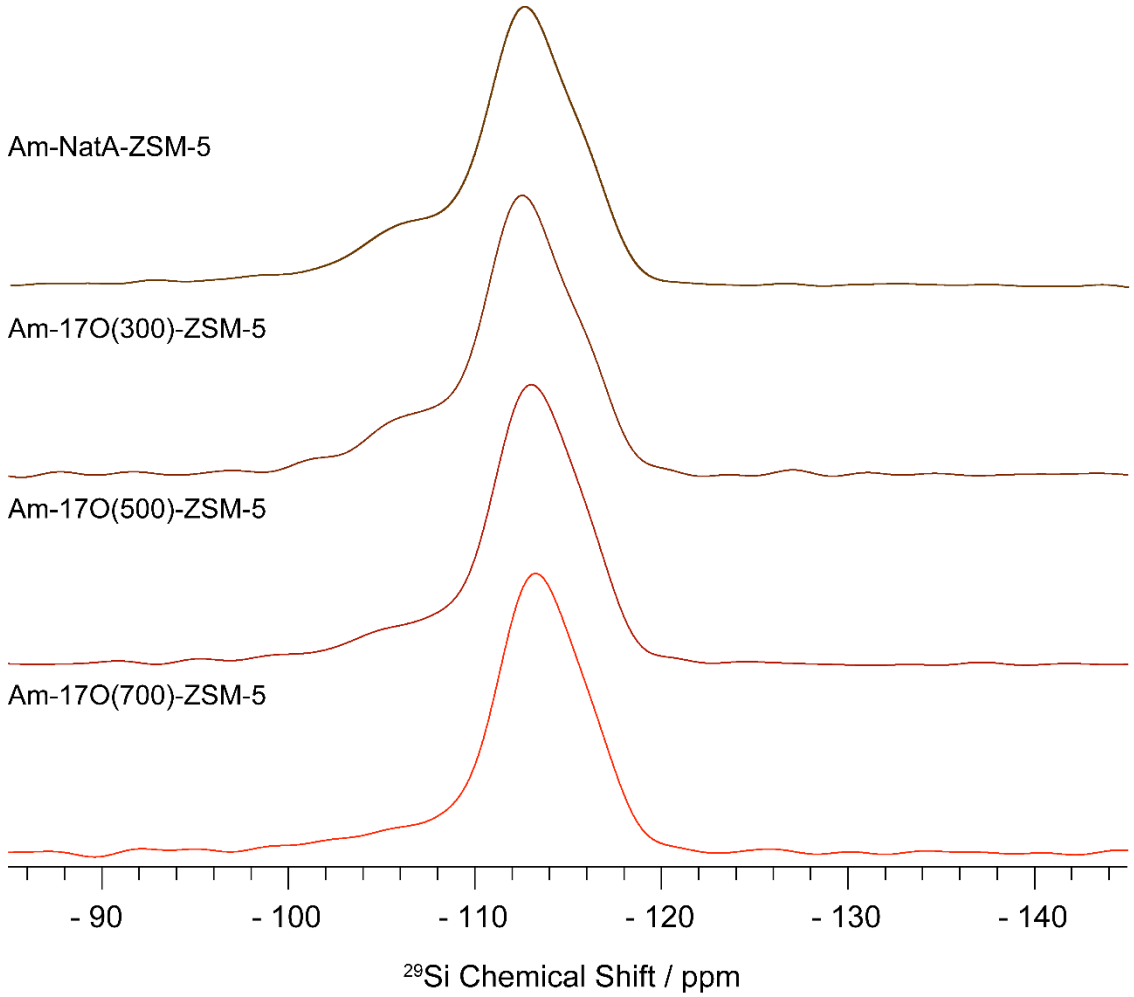

Figure S12. ^{29}Si MAS NMR spectrum of Am-NatA-ZSM-5 and after ^{17}O enrichment at various temperatures as indicated. Data were acquired at B_0 = 9.4 T and with ν_r = 10 kHz.

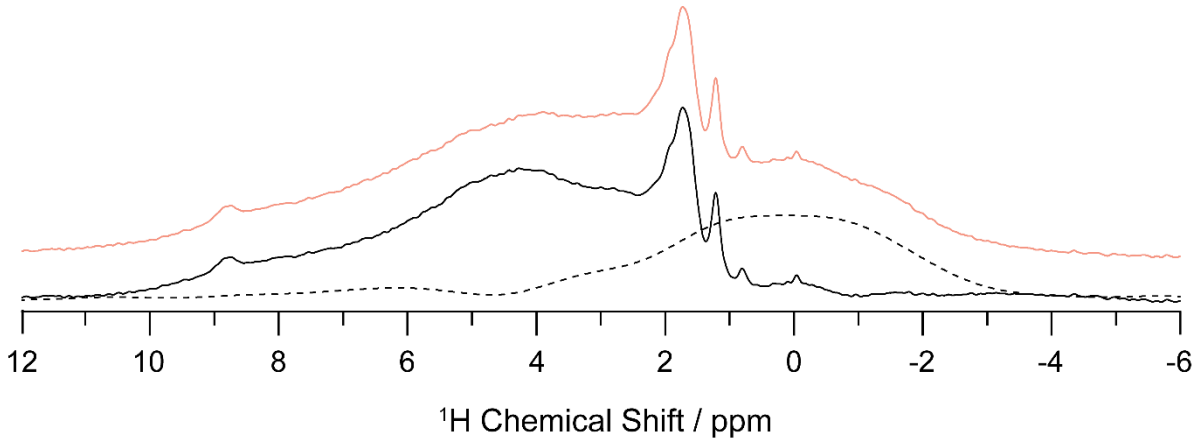

Figure S13. ^{1}H MAS NMR spectra acquired at B_0 = 20.0 T and with ν_r = 16 kHz for De-NatA-ZSM-5 (orange) and an empty rotor (black dashed line). The difference (black solid line) between the sample and background spectra is also shown for illustration.

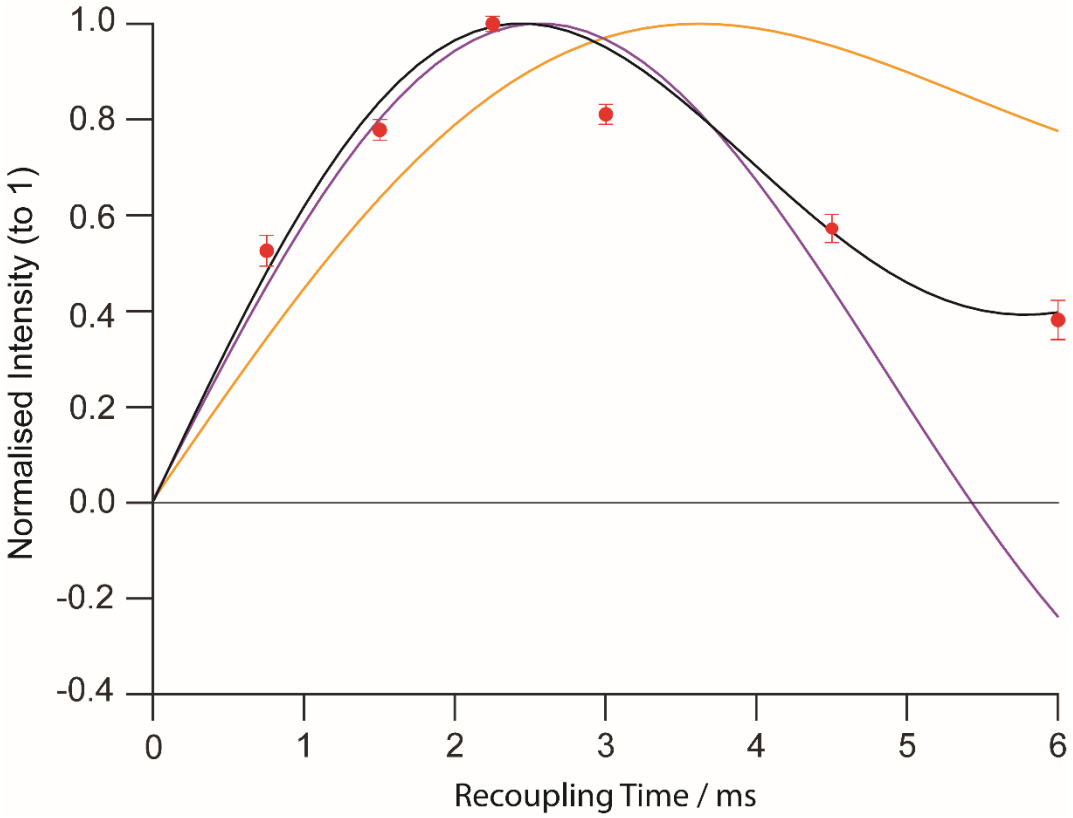

Figure S14. ^{1}H signal amplitude build-up curves of Act-^{17}O(500)-ZSM-5 in the 2D ^{1}H-^{17}O HMQC spectra (at ^{17}O shift = 30 ppm) as a function of recoupling times for signal at 6.9 ppm (red points). A SIMPSON numerical simulation of the build-up curve for a two-spin ^{1}H-^{17}O system with a dipolar coupling constant of 100 Hz is shown with a purple line. Further simulations with an additional ^{1}H spin with a dipolar coupling constant of 300 Hz and a ^{1}H-^{17}O dipolar coupling constant of 100 and 130 Hz are shown with yellow and black lines respectively.

A simpler two-spin model with a ^{1}H-^{17}O dipolar coupling constant of 100 Hz (Figure S14, purple) adequately reproduces the initial build-up but exhibits a substantially faster decay than observed experimentally. The incorporation of a second ^{1}H spin, dipolar-coupled (300 Hz) to the primary ^{1}H, significantly improves the agreement between simulation and experiment, highlighting the importance of homonuclear proton-proton interactions in modulating the D-HMQC transfer efficiency.

References

1. T. C. Hoff, R. Thilakaratne, D. W. Gardner, R. C. Brown and J.-P. Tessonnier, Thermal stability of aluminum-rich ZSM-5 zeolites and consequences on aromatization reactions, *J. Phys. Chem. C*, 2016, **120**, 20103–20113.
2. U. Schwerk and D. Michel, ^{1}H NOESY NMR on adsorbed molecules, *J. Phys. Chem.*, 1996, **100**, 352–356.
3. B. M. Fung, A. K. Khitrin and K. Ermolaev, An improved broadband decoupling sequence for liquid crystals and solids, *J. Magn. Reson.*, 2000, **142**, 97–101.
4. A. Medek, J. S. Harwood and L. Frydman, Multiple-quantum magic-angle spinning NMR: A new method for the study of quadrupolar nuclei in solids, *J. Am. Chem. Soc.*, 1995, **117**, 12779–12787.
5. J.-P. Amoureux, C. Fernandez and S. Steuernagel, ZFiltering in MQMAS NMR, *J. Magn. Reson., Ser. A*, 1996, **123**, 116–118.
6. Y. Millot and P. P. Man, Procedures for labeling the high-resolution axis of two-dimensional MQ-MAS NMR spectra of half-integer quadrupole spins, *Solid State Nucl. Magn. Reson.*, 2002, **21**, 21–43.
7. O. Lafon, Q. Wang, B. Hu, F. Vasconcelos, J. Trébosc, S. Cristol, F. Deng and J.-P. Amoureux, Indirect detection via spin-1/2 nuclei in solid state NMR spectroscopy: Application to the observation of proximities between protons and quadrupolar nuclei, *J. Phys. Chem. A*, 2009, **113**, 12864–12878.
8. C. R. Morcombe and K. W. Zilm, Chemical shift referencing in MAS solid state NMR, *J. Magn. Reson.*, 2003, **162**, 479–486.
9. E. Lippmaa, M. Maegi, A. Samoson, M. Tarmak and G. Engelhardt, Investigation of the structure of zeolites by solid-state high-resolution ^{29}Si NMR spectroscopy, *J. Am. Chem. Soc.*, 1981, **103**, 4992–4996.
10. M. Bak, J. T. Rasmussen and N. C. Nielsen, SIMPSON: A general simulation program for solid-state NMR spectroscopy, *J. Magn. Reson.*, 2000, **147**, 296–330.
11. D. Iuga, E. K. Corlett and S. P. Brown, ^{35}Cl–^{1}H Heteronuclear correlation magic-angle spinning nuclear magnetic resonance experiments for probing pharmaceutical salts, *Magn. Reson. Chem.*, 2021, **59**, 1089–1100.
12. J. M. Koons, E. Hughes, H. M. Cho and P. D. Ellis, Extracting multitensor solid-state NMR parameters from lineshapes, *J. Magn. Reson., Ser. A*, 1995, **114**, 12–23.